

# EVENT RATES AND TIMESCALE DISTRIBUTIONS FROM REALISTIC MICROLENSING MODELS OF M31

EDWARD A. BALTZ<sup>1</sup>, GEZA GYUK<sup>2,3</sup> AND ARLIN CROTTS<sup>1</sup>

1. ISCAP, Columbia Astrophysics Laboratory, 550 W 120th St., Mail Code 5247, New York, NY 10027

2. Department of Astronomy and Astrophysics, University of Chicago, Chicago, IL 60637

3. Adler Planetarium and Astronomy Museum, Chicago, IL 60605

*Draft version October 24, 2018*

## ABSTRACT

We provide a set of microlensing event rate maps for M31, the Andromeda Galaxy. Rates for M31 microlensing were calculated on the basis of a four component model of the lens and source populations: disk and bulge sources lensed by bulge, disk, M31 halo and Galactic halo lenses. We confirm the high rate gradient along the minor axis of M31 due to a dark halo of lenses. Furthermore, we compute the timescale distributions of events, for both Einstein times and full-width at half-maximum times. We explore how the rate contours and the timescale distributions can be used to measure the shape and extent of the microlensing halo. With one year of twice-weekly sampling, or three observing seasons, a halo MACHO fraction as small as 5% can be detected with modest ground based telescopes.

*Subject headings:* gravitational lensing

## 1. INTRODUCTION

Gravitational microlensing as a means to detect compact objects in the Galactic halo was first considered by Paczyński (1986), but the basic idea is much older (Einstein 1936). This suggestion was realized as results from two surveys of microlensing events towards the Large and Small Magellanic Clouds (LMC and SMC) (Alcock et al. 2000; Ansari et al. 1996). These were consistent with a significant, but subdominant, contribution of microlensing masses to the Galactic dark matter halo. Nonetheless, these conclusions are still controversial, and the identity and location of the microlensing masses are still mysterious.

A decade ago, M31 was suggested as a promising venue where galactic microlensing might be explored in ways advantageous and distinctive from that in and around the Galaxy (Crotts 1992). Several papers (Jetzer 1994; Han & Gould 1996; Baltz & Silk 2000; Kerins et al. 2001) have confirmed that a substantial microlensing signal can be expected. Two collaborations, MEGA (preceded by the VATT/Columbia survey) and AGAPE have produced a number of microlensing event candidates involving stars in M31 (Crotts & Tomaney 1996; Ansari et al. 1999, Aurière et al. 2001, Uglesich 2001, Calchi Novati et al. 2002). Here we show the potential for these and future surveys to settle some of the outstanding questions regarding microlensing in spiral galaxies.

This is the second paper in a series. Paper I (Gyuk & Crotts 2000) provides optical depth maps for M31. While these are useful tools for certain purposes they are unfortunately not directly measurable. Event rates on the other hand *are* directly measurable and hence their magnitude and variation across the face of M31 are more meaningful in planning and evaluating surveys of microlensing. In this paper we extend Paper I to include event rate maps, both total and also differential rates with respect to the event timescale.

This paper is organized as follows. In §2 we briefly discuss the M31 models we used, including disk, bulge and

halo components. Following this we present rate maps for various halo models, including the self lensing contribution, in §3. In §4 we provide differential rate distributions as a function of two different timescale measures, and we discuss how cuts in timescale can be used to separate self lensing from a MACHO halo contribution to the lensing rate. We conclude with a discussion of measuring lens masses and halo properties in §5.

## 2. MODELING

The execution of a microlensing survey of M31 is qualitatively different from those towards the Magellanic Clouds or our own Galactic bulge. For the latter, individual stars can often be resolved, and their unlensed fluxes measured, admitting a direct measurement of the magnification during a microlensing event. In contrast, M31 is more than ten times farther away, and individual stars are rarely resolved from the ground. Images are almost always highly crowded, and individual sources are almost always highly blended. This is the “pixel lensing” regime (Crotts 1992; Baillon et al. 1993). Image subtraction, necessitated by the high degree of crowding, has been very successful. While this technique allows the detection of variable objects of any kind, and is photon noise limited, the unlensed fluxes of lensed sources are unknown. Thus M31 microlensing surveys must make do with a full width at half maximum timescale and a flux increase at maximum as the useful fit parameters. The unlensed flux measured by classical microlensing surveys is unavailable under most circumstances.

Sources are taken to reside in a luminous two-component model of M31 consisting of a double exponential disk and a bulge. The disk model is inclined at an angle of  $77^\circ$  and has a scale radius of 5.98 kpc, a scale height of 400 pc, a central surface brightness of  $\mu_R = 20$ ,  $V - R = 0.67$ , and we ignore spiral arm effects (Walterbos & Kennicutt 1988; Gould 1994). We take an  $I$  band surface brightness profile from the  $V - R$  color and the observation that  $V - R \approx R - I$  (Bessel 1979). The rota-

tion velocity is taken to be  $240 \text{ km s}^{-1}$ , with a linear rise from the center to 6 kpc. The bulge model is based on the “small bulge” of Kent (1989) with a central surface brightness of  $\mu_R = 14$ , and  $R - I = 0.72$  (Walterbos & Kennicutt 1988; Bessel 1979). This is an axisymmetric bulge with a roughly  $\exp(-r^{0.4})$  falloff in volume density with an effective radius of approximately 1 kpc and axis ratio,  $c/a \sim 0.8$ . Values of the bulge density are normalized to make  $M_{\text{bulge}} = 4 \times 10^{10} M_{\odot}$ . The velocity distribution of bulge stars is taken to be maxwellian ( $dN \propto \exp(-v^2/2\sigma^2)d^3v$ ), with  $\sigma = 150 \text{ km s}^{-1}$ . These quantities are fairly well known, and unlikely to change the results by a large amount if revised.

We explore a parameterized set of M31 halo models. Each model halo is an axisymmetric cored “isothermal sphere” determined by two parameters: the axis ratio or flattening  $q$  (where  $q = 1$  indicates no flattening) and the core radius  $r_c$ . As we are concerned with lensing objects we also define the MACHO fraction ( $f_b$ ) as the fraction of the halo mass that consists of lensing objects. Together, the mass density of halo lensing objects is then

$$\rho(x, y, z) = f_b \frac{V_c(\infty)^2}{4\pi G} \frac{e/(q \sin^{-1} e)}{x^2 + y^2 + (z/q)^2 + r_c^2}, \quad (1)$$

where  $e = \sqrt{1 - q^2}$  and  $V_c(\infty) = 240 \text{ km s}^{-1}$  is taken from observations of the M31 disk. The velocity distribution of the halo is taken to be maxwellian, with a circular velocity equal to  $V_c(\infty)$ , making  $\sigma = 170 \text{ km s}^{-1}$ .

We compute rate distributions with respect to two different timescales. The first is the more familiar Einstein time ( $t_E$ ), defined as the time to cross the full Einstein disk which has radius

$$R_E = \sqrt{\frac{4GM_{\text{lens}}D_s x(1-x)}{c^2}}, \quad (2)$$

where  $x$  is the fractional distance to the lens in relation to the distance to the source,  $D_s$ . The Einstein time is then given in terms of the lens velocity perpendicular to the line of sight,

$$t_E = \frac{2R_E}{v_{\perp}}. \quad (3)$$

The second timescale we use is the full-width at half maximum of the lightcurve  $t_{1/2}$ , much more easily measured when the source fields are crowded, as is the case for M31. This timescale is simply related to the Einstein time and to the minimum impact parameter  $\beta$  of the lens relative to the line of sight (taken in units of  $R_E$ ). This timescale is given by (Gondolo 1999)

$$t_{1/2} = t_E w(\beta), \quad (4)$$

with the following definitions

$$w(\beta) = \sqrt{2f(f(\beta^2)) - \beta^2}, \quad f(x) = \frac{2+x}{\sqrt{x(4+x)}} - 1. \quad (5)$$

The function  $w(\beta) \sim \beta$  for all values of  $\beta$ , with the limiting behavior

$$w(\beta \ll 1) \approx \beta\sqrt{3}, \quad w(\beta \gg 1) \approx \beta\sqrt{2} - 1. \quad (6)$$

Thus,  $t_{1/2} \sim \beta t_E$ , and is more degenerate than  $t_E$  due to the dependence on impact parameter. A further complication is that  $t_{1/2}$  is essentially the measured timescale. Determining the Einstein time requires knowledge of the magnification, which can be very difficult

in highly crowded fields as the source stars are highly blended. The Einstein time might be inferred with extra effort, either by high resolution imaging of the source star or statistically with the  $t_{\sigma}$  technique (Baltz & Silk 2000). It is crucial to evaluate if these are necessary.

### 3. RATE MAPS

Using the model of §2, we compute the rate of detectable microlensing events. Two computer codes written entirely independently and described elsewhere (Baltz & Silk 2000; Gyuk & Crotts 2000) have been used, and produce nearly identical results. A numerical integration of the rate is performed, over the positions and velocities of the source (with fixed brightness) and lens (with fixed mass) along a given line of sight. The probability that an event with given parameters is detected is folded into the integral. Mass functions for the lenses and luminosity functions for the sources are applied at the end.

With lines of sight spaced at one arcminute intervals, we construct contour maps of the event rate for “self lensing” by stars (assuming no binary lenses, at most a 15% contribution (Mao & Paczyński 1991; Baltz & Gondolo 2001)) as well as for halo lensing. The self lensing contribution has four logical contributions, taking sources and lenses from the bulge and disk. The bulge-bulge contribution dominates the self lensing near the center of the bulge, along the minor axis the bulge-disk and disk-bulge contributions dominate, and far from the bulge the disk-disk contribution dominates (though this is always dominated by the halo contribution for  $f_b > 0.05$ ). These four in sum give a self lensing rate that is nearly symmetric about both the major and minor axes of M31. The halo lensing contributions arise from both the M31 and Milky Way halos, lensing both disk and bulge stars. The Milky Way contribution has a nearly uniform optical depth. The M31 contribution is strongly asymmetric, with a significantly larger rate from the far edge of the minor axis.

We have assumed the following definition for a detectable microlensing event. The MEGA survey most frequently employs the MDM 2.4m telescope, thus we use its capabilities in the following. We assume that integrations totaling three hours are taken twice weekly during the M31 observing season: this is fairly conservative. We define an event as a deviation that has two consecutive samples four standard deviations above the baseline. We assume one arcsecond seeing, which is typical: the median MDM seeing is 0.95 arcsecond. To approximate the sensitivity of MDM, we assume that a star of  $R$  magnitude  $m_R = 25.2$  or  $I$  magnitude  $m_I = 24.8$  gives one photoelectron per second, and furthermore that the noise in the images is twice the photon counting noise (this is quite conservative). We take the distance modulus to M31 as  $D = 24.5$ , a distance of 795 kpc. We assume a sky brightness of  $\mu_R = 21$  and  $\mu_I = 20 \text{ mag arcsec}^{-2}$ . Here we reiterate the fact that the source stars are not resolved, but instead are typically *highly* blended. Only with difference imaging can the microlens variability be detected. The only measured “baseline flux” is the light falling within a resolution element due to several stars in the highly crowded fields.

The luminosity function of M31 sources must be specified. For the disk, we take  $R$  and  $I$  band luminosity functions from Mamon & Soneira (1982). For the bulge,

we take the  $I$  band from Terndrup, Frogel & Whitford (1990). Data for the  $R$  band is scarce, so we average (in  $\log dN/dM$ )  $V$  and  $I$  band data for  $M_R > 0$  (using Terndrup et al. (1990) for  $I$  and Holtzman et al. (1998) for  $V$ ). For  $M_R < 0$  we attach a power law slope of 0.59 taken from the MACHO project data (Alves 2001).

The mass function of lenses, both stellar and the MACHO component, is somewhat problematic. For the stellar component, we use the exponential Chabrier (2001) mass function, down to  $0.01M_\odot$ . This is steeply decreasing, so there is little mass in the lowest decade (the brown dwarfs). Varying the stellar mass function in acceptable ranges has little effect unless for example there is a large component of brown dwarfs (Baltz & Silk 2001). The mean stellar mass of about  $0.5M_\odot$  is what dominates the rate and timescale from self lensing. We have also investigated a Scalo (1986) mass function, which has a slightly higher mean mass, thus longer timescales and lower rates. The differences are not very large however. For lack of convincing evidence to the contrary, we take a fixed mass for MACHOs. Based on Alcock et al. (2000) we assume a mass of  $-3/8$  dex relative to solar ( $\approx 0.422M_\odot$ ), and we test values of  $0.1M_\odot$  and  $1.0M_\odot$  as well. We note here that MACHO mass can have a large effect on the expected timescales and rates. Larger masses would indicate a lower rate and longer events, while smaller masses give a higher rate but shorter events. This is discussed further in the next section.

In Figs. 1-6 we plot event rate contours for  $R$  band observations. The contours for  $I$  band are very similar. The only pronounced difference is in the bulge, where the  $I$  band luminosity function is quite shallow, there is a significantly larger rate in the most central 4 square arcminutes. While it is desirable to detect events in two bands to test that the flux *enhancement* has a constant color (in time), as should be the case for gravitational lensing, we will not include this criterion. The separate event rates are very similar, thus we deem it unlikely that the joint event rate will be much different. In Fig. 1 we plot the rate contours for self lensing and for M31 halos with a 20% MACHO fraction c.f. Alcock et al. (2000) ( $f_b = 0.2$ ) and a core radius of 2 kpc. Both round ( $q = 1$ ) and flattened ( $q = 0.3$ ) halos are illustrated. These maps are given as contours of constant rate, in units of events  $\text{yr}^{-1} \text{ arcmin}^{-2}$ . In Fig. 2 we plot rate contours again for  $f_b = 0.2$ , but compare the small ( $r_c = 1$  kpc) and large ( $r_c = 5$  kpc) core cases, for both round and flattened halos. In Fig. 3 we illustrate the event rate from Milky Way MACHOs, assuming both round and flattened cases again. The rate should be related to the surface brightness, also illustrated. In fact a naive calculation indicates that the rate from a constant optical depth of lenses (such as a Milky Way population, which wouldn't vary much over the M31 fields) should be proportional to the square root of the surface brightness. This can be seen from the following simple argument. The number of monitored sources is proportional to the surface brightness (the proportionality constant depends on luminosity function), but the noise level increases as the square root of the surface brightness, necessitating an increase in magnification by the same factor to obtain an equivalent signal to noise. Since the peak magnification of the event is proportional to the inverse of the impact parameter, the total cross section goes down by this square root of sur-

face brightness. Thus, the number of monitored sources times the cross section is proportional to the square root of the surface brightness. This argument breaks down at very high surface brightness where the magnification required implies events whose full width at half maximum timescales are too short to detect, however, this regime is not reached for M31 for the masses assumed. From Fig. 3 we see that this calculation is reasonable, as the shape of rate contours matches the shape of the surface brightness contours, and the rate of decline is roughly half on the logarithmic scale illustrated. The flattening of the Milky Way halo only changes the normalization of the rates, not the shape of the contours.

Combining all of these components, we illustrate the total expected event rate. In the bottom panel of Fig. 4, we plot contours of the total microlensing rate, from self lensing and 20% MACHO halos for both the Milky Way and M31. The self lensing dominates in the inner 5 kpc, but outside, the 20% halo provides most of the events. Changing the halo fraction  $f_b$  has little effect on the shape of the contours, and only in the region where the self lensing and halo lensing are comparable (roughly speaking within the  $0.3 \text{ events arcmin}^{-2} \text{ yr}^{-1}$  contour assuming a 20% halo). The overall normalization of the event rate away from the bulge can give a clear measurement of  $f_b$ . For example, comparing a 20% halo to the case of a 5% halo, the inner contours (within  $1 \text{ event arcmin}^{-2} \text{ yr}^{-1}$ ) are not much affected since self lensing dominates and the *shape* of the outer contours is very similar since it is the halo that dominates there in both cases. Between the 1.0 and 0.3 contours the event rate drops more quickly in the 5% halo case since this is the region where the microlensing rate from the halo and stellar components are comparable. This is clear from inspecting the top panel of Fig. 1 (the self lensing rate) and comparing to the bottom panel (the M31 halo lensing rate) which is trivially rescaled according to MACHO fraction.

Fig. 4 shows the difference in the rate contours for round  $q = 1$  and flattened  $q = 0.3$  halos. The two cases appear to be easily distinguishable, especially along the major axis. In the bottom panel of Fig. 5, we again plot contours of the total microlensing rate, this time varying the halo core radius from 1, 2, 5, 10 kpc. The significant difference is on the far side, along the minor axis. A crude measurement of core radius may thus be possible.

Here we see the utility of using the raw event rates to determine parameters. We do not need to evaluate the optical depth to do so. Since in the end we are interested in the halo parameters like MACHO fraction and flattening, the optical depth is secondary.

#### 4. TIMESCALE DISTRIBUTIONS

The Einstein time is the fundamental timescale parameterizing the variability due to lensing, but it is notoriously difficult to measure from a pixel microlensing event. The directly measured parameter is the full-width at half-maximum timescale. We will illustrate the rate distribution of events in both of these timescales in Fig. 4, and we will discuss the extraction of halo parameters using both. The calculation of the differential rate with respect to  $t_{1/2}$  follows Baltz & Silk (2000), based on Griest (1991) who discusses the differential rate with respect to  $t_E$ . We plot

the differential rate with respect to the logarithm of the timescale, normalized by the differential rate at a fixed timescale  $\tilde{t}$ ,

$$\frac{d\tilde{\Gamma}}{d \log t} = \frac{d\Gamma}{d \log t} \bigg/ \frac{d\Gamma}{d \log t}(\tilde{t}). \quad (7)$$

Taking  $\tilde{t}$  longer than the the peak timescale then illustrates the variation in how rapidly the differential event rate falls at long timescales. In the upper panels of Fig. 4 we illustrate  $d\tilde{\Gamma}/d \log t$  for both  $t_E$  and  $t_{1/2}$ . For lines of sight far from the bulge, the distribution in  $t_{1/2}$  peaks at around 20 days, while the distribution of  $t_E$  peaks at around 100 days. Near the bulge, the peaks of both timescale distributions are shorter.

Away from the bulge, where MACHO events dominate, the peak timescale is a measurement of the MACHO mass, as  $t_E \propto \sqrt{M_{\text{lens}}}$ . Taking a single mass, the  $t_E$  distributions are  $\approx 0.5$  dex wide in  $t_E$ , translating to  $\approx 1.0$  dex wide in  $M_{\text{lens}}$ . With 50 events, a  $\pm 20\%$  measurement of the mass would be possible with known Einstein times. With only  $t_{1/2}$ , the situation is considerably worse, as the distribution in  $t_{1/2}$  for a fixed mass is  $\approx 1.0$  dex wide in  $t_{1/2}$ , thus  $\approx 2.0$  dex wide in  $M_{\text{lens}}$ . With the same 50 events, a mass measurement at the level of  $\pm 40\%$  can be made. We thus see the utility of determining the Einstein times for the events.

We expect MACHO events to have longer timescales than stellar events simply due to the geometry, i.e. the source–lens distances can be much larger. To compare, the bulge is of order 1 kpc in size, while a cored halo does not drop appreciably in density for of order 10 kpc. Halo lenses have a larger velocity dispersion than bulge lenses, but not by a large factor. In all, we might expect halo lens timescales to be a factor of 2.5 or so larger. This fact can be used to determine cuts in timescale, either  $t_E$  or  $t_{1/2}$ , that maximizes the possibility that MACHO events can be distinguished from stellar events. We want a cut that both excludes as many self lensing events as possible and includes as many MACHO events as possible. We thus wish to maximize the signal to noise, including both the Poisson counting of events, and a systematic error due to the uncertainty in the self lensing model. For a given area, observation time and minimum timescale, we expect  $N_{\text{M31}}$  events from M31 MACHOs,  $N_{\text{MW}}$  events from Milky Way MACHOs, and finally  $N_S$  events from stellar lenses, with an uncertainty of  $\Delta N_S$  (which we take to be  $0.3N_S$ ). We minimize the quantity

$$\frac{1}{Q^2} = \frac{N_{\text{M31}} + N_{\text{MW}} + N_S}{N_{\text{M31}}^2} + \left( \frac{\Delta N_S}{N_{\text{M31}}} \right)^2 \quad (8)$$

as a function of minimum timescale to determine what, if any, timescale cut to use. These results are plotted in the top panels of Fig. 5. For most of the field, we find that no timescale cut should be made. Near the center of the bulge, within 6 arcmin on the minor axis and 12 arcmin on the major axis, the situation is different. If the Einstein times are known, it is advantageous to cut all events with  $t_E < 75$  days. This allows the largest signal to noise for separating the halo component. Without the cut, for a one year survey the separation can be done at the  $2.5\sigma$  level over the interior region. With the cut, the significance rises to  $4\sigma$ . If only  $t_{1/2}$  is known, a similar timescale cut does not help much. We comment here that if we were to

take a more conservative value for the model uncertainty (say  $\Delta N_S = 0.5N_S$ ), the results are only affected near the center of the bulge, but the desired cutoff in Einstein time and the signal to noise for detecting a halo knowing the Einstein times are hardly affected even there. We also note that the utility of timescale cuts may change if the MACHO mass were to be significantly different from typical stellar masses. As it is now, the MACHO project mass value and the typical stellar mass are quite similar.

Over the full far–side MDM field, a microlensing halo for M31 can be detected at roughly  $7\sigma$  significance with one full year of well–sampled data, or approximately three observing seasons. This assumes  $f_b = 20\%$ , but the significance is roughly linear with  $f_b$ . For  $f_b = 10\%$ , a microlensing halo can be detected at roughly  $4\sigma$  significance, and with  $f_b = 5\%$ , the significance drops to about  $2.5\sigma$ . Thus,  $f_b = 5\%$  is about the limit of detectability for a microlensing halo with three seasons of observing. This 5% value is also a plausible lower limit to halo lensing, caused by a much greater number of stars in M31’s halo/spheroid than the Galaxy’s (Reitzel et al. 1998, scaled to produce a microlensing prediction using Alcock et al. 1997, Table 10).

Finally, we discuss the effects of varying the MACHO mass on the total and differential rates. The stellar mass function will remain that of Chabrier (2001). In the bottom panel of Fig. 6 rate contours are plotted for fixed MACHO masses (for both the M31 and Milky Way contributions) of  $1.0M_\odot$ ,  $-3/8$  dex solar, and  $0.1M_\odot$ . As expected, the lower masses give larger rates. We have also given the MACHOs a Chabrier (2001) function, identical to the stars. The resulting rates are similar to the  $0.1M_\odot$  case (as the Chabrier mass function peaks there), thus we do not illustrate them. In the top panels of Fig. 6 we show  $d\tilde{\Gamma}/d \log t_{1/2}$  for lens masses of  $1.0M_\odot$  and  $0.1M_\odot$ . The shift in peak is clearly seen, as is the higher rate for smaller lenses. Taking a Chabrier (2001) mass function, the rate distribution is very similar to the fiducial case illustrated in Fig 4.

## 5. DISCUSSION

We have provided maps of the microlensing event rate towards M31 in a model including M31 disk and bulge sources, and lenses from the M31 disk and bulge, as well as lenses in the dark halos of M31 and the Milky Way. We have varied the parameters of the dark halo, namely the core radius and the flattening, and studied the effects on the rate contours. The core radius affects the rates most in the galaxy center but these changes are partially obscured by the high rate of self lensing events there. The flattening does have a significant effect, especially along the major axis. The normalization of the rate contours away from the bulge gives a measure of the halo MACHO fraction.

The easily measured timescale parameter is the full width at half maximum, but the more physical timescale is the Einstein time. Knowing the Einstein times allows a much more accurate measurement of the lens mass, thus it is worth the extra trouble to try to measure the Einstein times of the detected events.

We have shown that a microlensing halo in M31 should be clearly distinguishable from self lensing if an appreciable event rate away from the M31 bulge is measured. We

have explored the use of cuts in event timescale to separate the self lensing component from the halo lensing component of the event rate, and found that this helps near the bulge, but not further away. We have quantified the level of halo that is detectable, and found that a marginal detection of a 5% microlensing halo would be possible in three seasons of ground-based observations. Higher halo fractions can be detected more convincingly of course.

We wish to thank David Alves, Krzysztof Stanek and Larry Widrow for useful conversations. E.B. acknowledges support from the Columbia University Academic Quality Fund. G.G. wishes to acknowledge financial support from the Brinson Foundation. A.C. was supported by grants from NSF (AST 00-70882 and 98-02984) and STScI (GO-7376).

#### REFERENCES

- Alcock, C., et al. 1997, *ApJ*, 486, 697  
 Alcock, C. et al. 2000, *ApJ*, 542, 281  
 Alves, D. R. 2001, private communication  
 Ansari, R., et al. 1996, *A&A*, 314, 94  
 Ansari, R., et al. 1999, *A&A*, 344, L49  
 Aurière, M., et al. 2001, *ApJ*, 553, L137  
 Baillon, P., Bouquet, A., Giraud-Héraud, Y., & Kaplan, J. 1993, *A&A*, 277, 1  
 Baltz, E. A. & Gondolo, P. 2001, *ApJ*, 559, 41  
 Baltz, E. A. & Silk, J. 2000, *ApJ*, 530, 578  
 Baltz, E. A. & Silk, J. 2001, *MNRAS*, 323, L31  
 Bessell, M. S. 1979, *PASP*, 91, 589  
 Calchi Novati, S., et al. 2002, *A&A*, 381, 848  
 Chabrier, G. 2001, *ApJ*, 554, 1274  
 Crotts, A. P. S. 1992, *ApJ*, 399, L43  
 Einstein, A. 1936, *Science*, 84, 506  
 Gondolo, P. 1999, *ApJ*, 510, L29  
 Gould, A. 1994, *ApJ*, 435, 573  
 Griest, K. 1991, *ApJ*, 366, 412  
 Gyuk, G. & Crotts, A. 2000, *ApJ*, 535, 621  
 Han, C. & Gould, A. 1996, *ApJ*, 473, 230  
 Holtzman, J. A., Watson, A. M., Baum, W. A., Grillmair, C. J., Groth, E. J., Light, R. M., Lynds, R., & O'Neil, E. J. 1998, *AJ*, 115, 1946  
 Jetzer, P. 1994, *A&A*, 286, 426  
 Kent, S. M. 1989, *AJ*, 97, 1614  
 Kerins, E. et al. 2001, *MNRAS*, 323, 13  
 Mamon, G. A. & Soneira, R. M. 1982, *ApJ*, 255, 181  
 Mao, S. & Paczyński, B. 1991, *ApJ*, 374, L37  
 Paczyński, B. 1986, *ApJ*, 304, 1  
 Reitzel, D.B., Guhathakurta, P. & Gould, A. 1998, *AJ*, 116, 707  
 Scalo, J. M. 1986, *Fundamentals of Cosmic Physics*, 11, 1  
 Terndrup, D. M., Frogel, J. A., & Whitford, A. E. 1990, *ApJ*, 357, 453  
 Uglesich, R. 2001, Ph.D. thesis, Columbia University  
 Walterbos, R. A. M. & Kennicutt, R. C. 1988, *A&A*, 198, 61

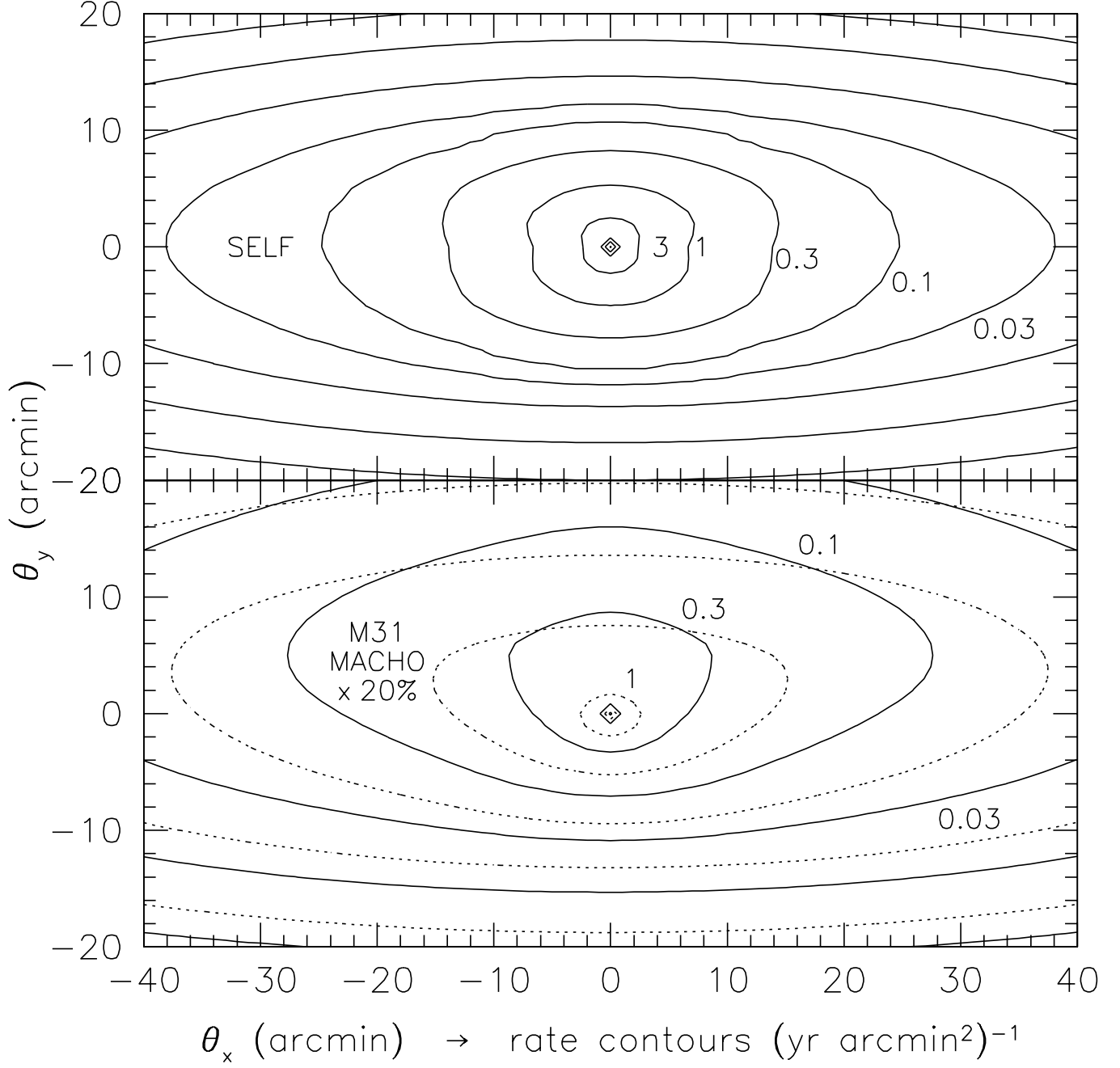


FIG. 1.— Rate contours for self lensing and M31 MACHO halos, in units of events per year per square arcminute. The top panel shows the self lensing component only, while the bottom panel shows the contribution of halo lensing with  $f_b = 0.2$  and  $r_c = 2$  kpc. The solid contours indicate a round ( $q = 1$ ) halo for M31, while the dotted contours indicate a flattened ( $q = 0.3$ ) halo. The number “3” in the contour labels should be taken as  $\sqrt{10}$ , i.e. the contours are separated by 0.5 dex in units of events  $\text{yr}^{-1} \text{ arcmin}^{-2}$ . The rate contours for self lensing are basically symmetric from front to back, since the disk provides an asymmetrical source population for bulge lenses, but also an asymmetrical lens population for bulge sources. We see the strong asymmetry in the rate of MACHO events.

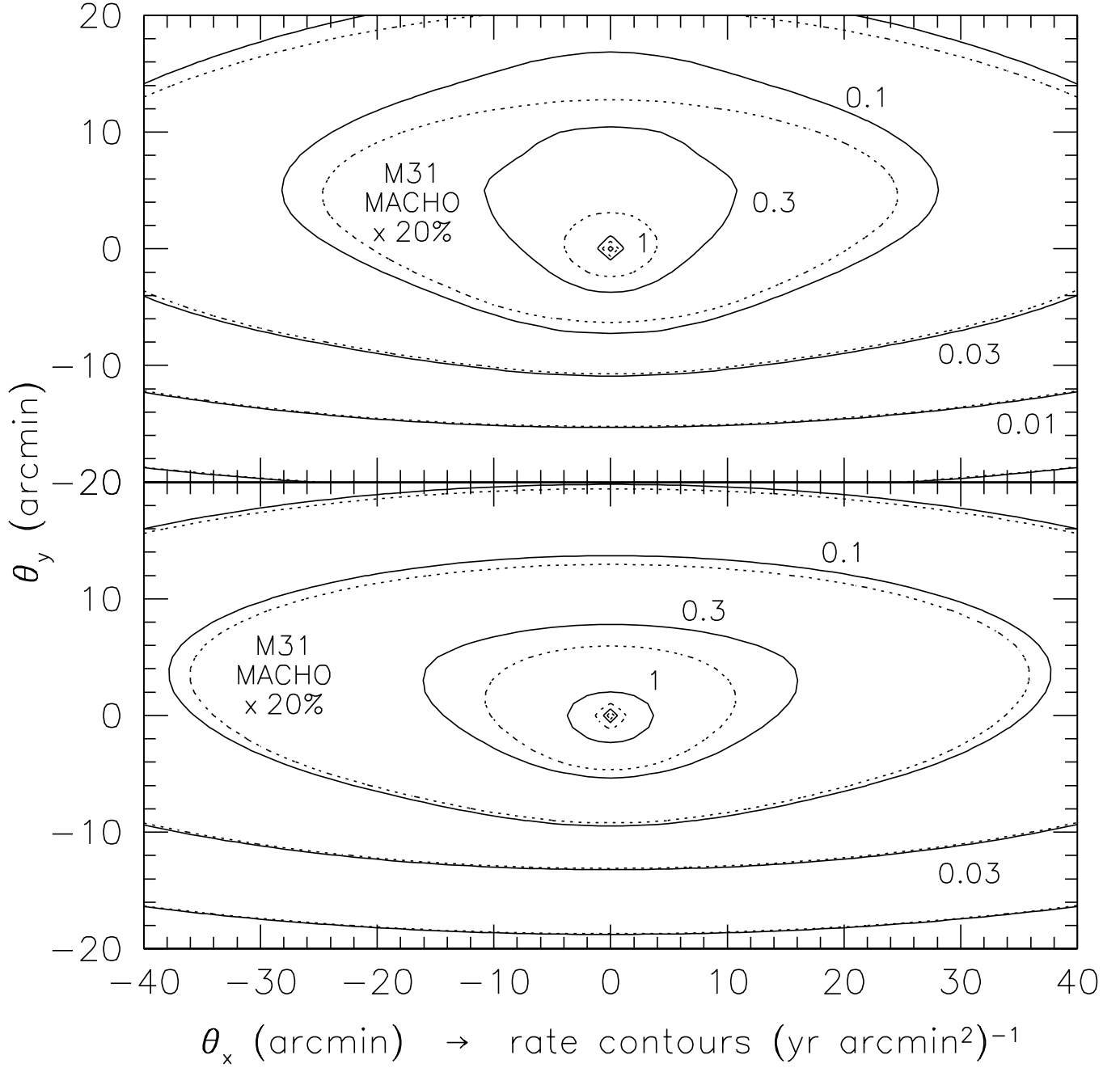


FIG. 2.— Rate contours for M31 MACHO halos, in units of events per year per square arcminute. All halos are taken with  $f_b = 0.2$ . The top panel shows halo lensing for a round ( $q = 1$ ) halo, while the bottom panel shows the contribution of a flattened ( $q = 0.3$ ) halo. The solid contours indicate  $r_c = 1$  kpc, while the dotted contours indicate  $r_c = 5$  kpc. The labels are as Fig. 1. It is evident that measuring the core radius from microlensing will be difficult, especially in the case of a flattened halo.

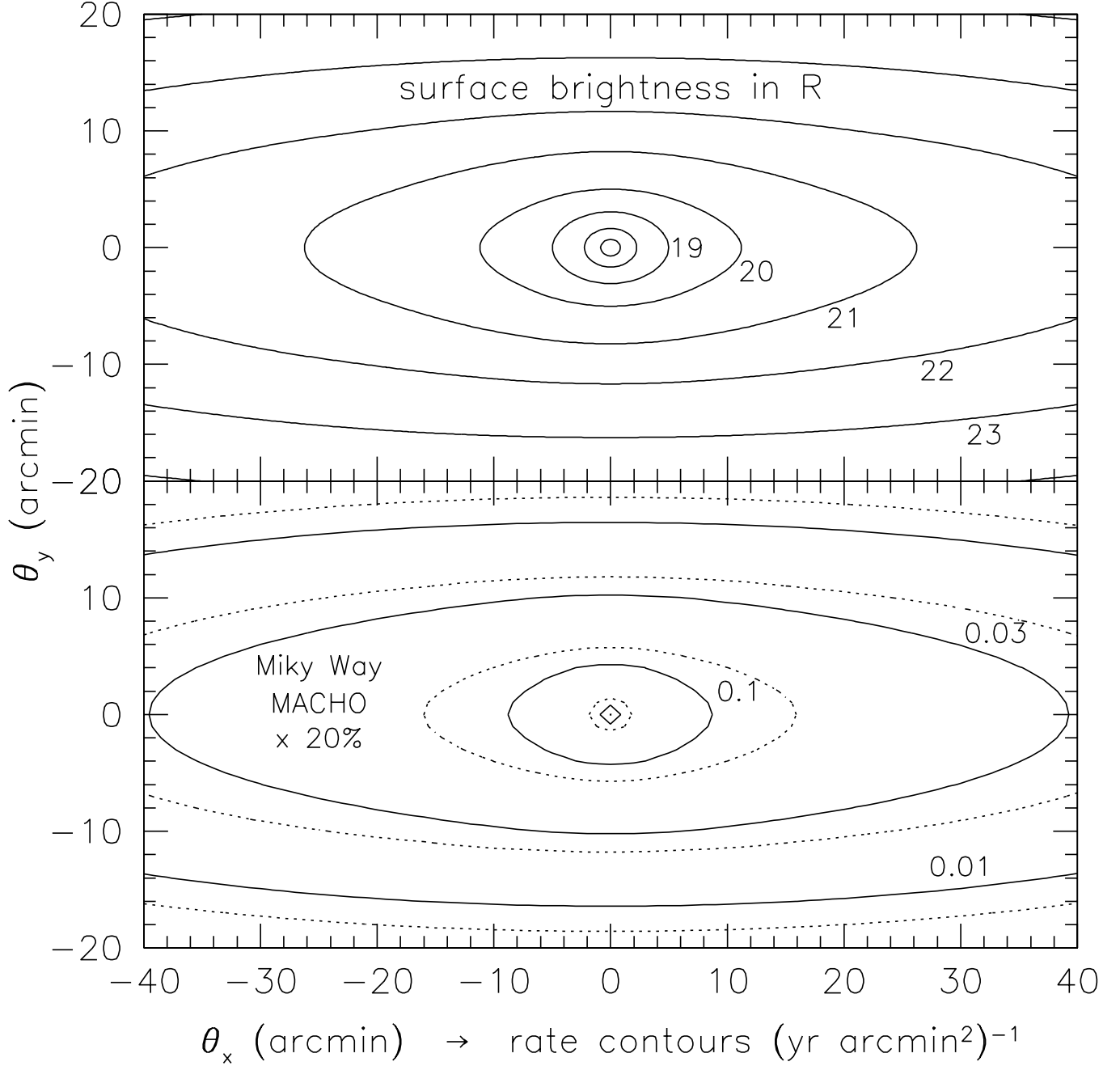


FIG. 3.— Surface brightness and rates for Milky Way MACHOs. The surface brightness is given in  $R$  magnitudes per square arcsecond. The Milky Way MACHO rates are given in units of events per year per square arcminute. The halos are taken with  $f_b = 0.2$ . The top panel illustrates the surface brightness contours. The bottom panel illustrates the rates, with a  $q = 1$  halo in solid contours and a flattened  $q = 0.3$  halo in dotted contours. The labels are as Fig. 1. The optical depth to Milky Way lensing is quite uniform across M31, thus the rate only tracks the surface brightness, as expected.



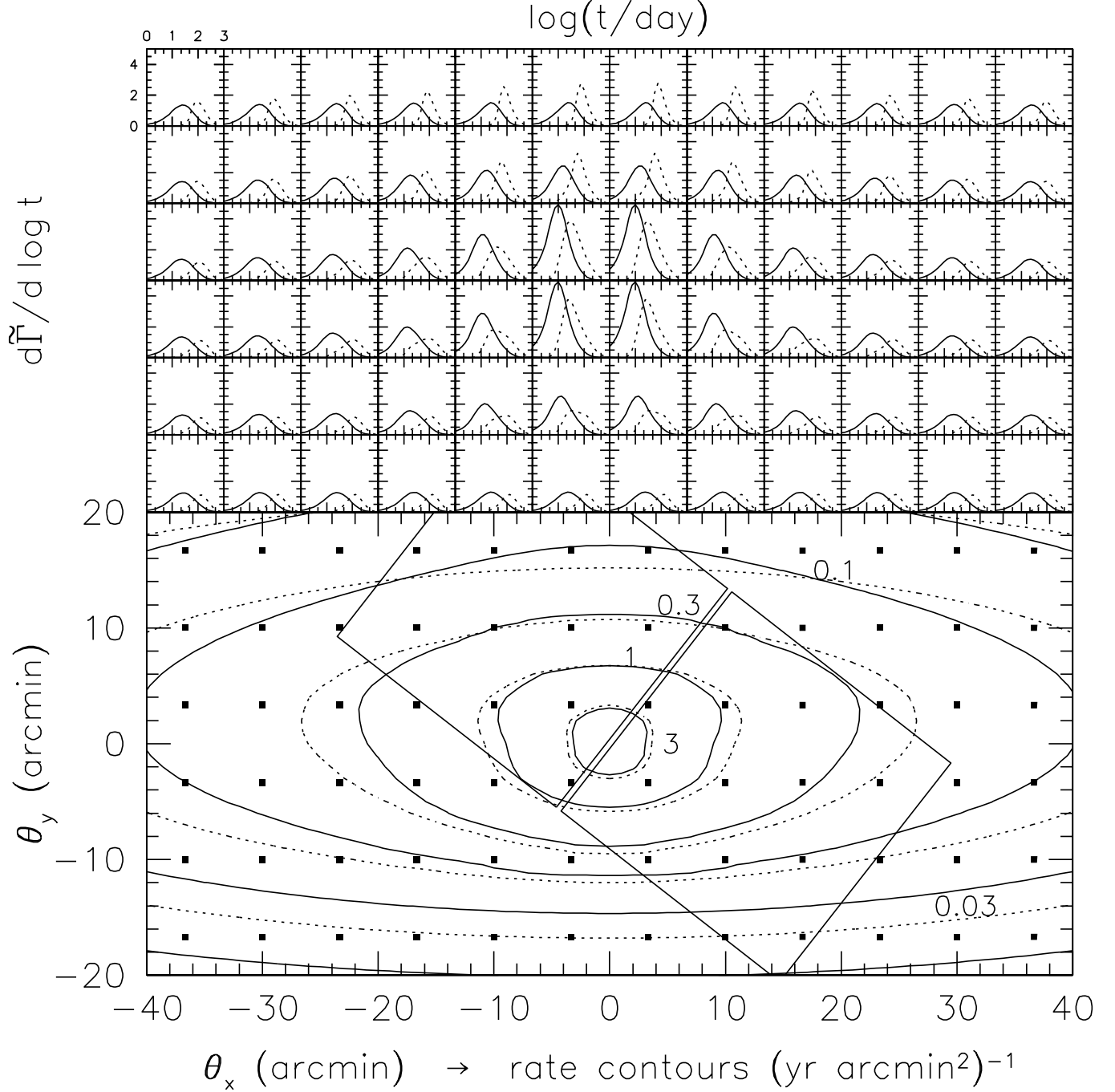


FIG. 4.— Rate contours for microlensing for different halo flattening values (in units of events per year per square arcminute) and rate distributions for two timescale measures. The bottom panel illustrates the  $f_b = 0.2$ ,  $r_c = 2$  kpc case, with solid contours indicating  $q = 1$ , and dotted contours indicating  $q = 0.3$ . The self lensing and Milky Way contributions are included. Self lensing is dominant through most of the central region (with 5 arcmin of the center). The square MDM fields are illustrated. The dots on the contour plot indicate the lines of sight where we illustrate the distribution of timescales  $d\tilde{\Gamma}/d \log t$  in the small top panels. The solid curves are for  $t_{1/2}$ , while the dotted curves are for  $t_E$ , both for the  $q = 1$  halo, though the differences between that and the  $q = 0.3$  case are slight. The  $t_{1/2}$  plots are normalized to unity at  $\log(\tilde{t}_{1/2}/\text{day}) = 1.75$  (about 56 days), while the  $t_E$  plots are normalized at  $\log(\tilde{t}_E/\text{day}) = 2.25$  (about 178 days). We thus see the variation in the long timescale tail across the image. In the central region the differential rate drops more quickly.

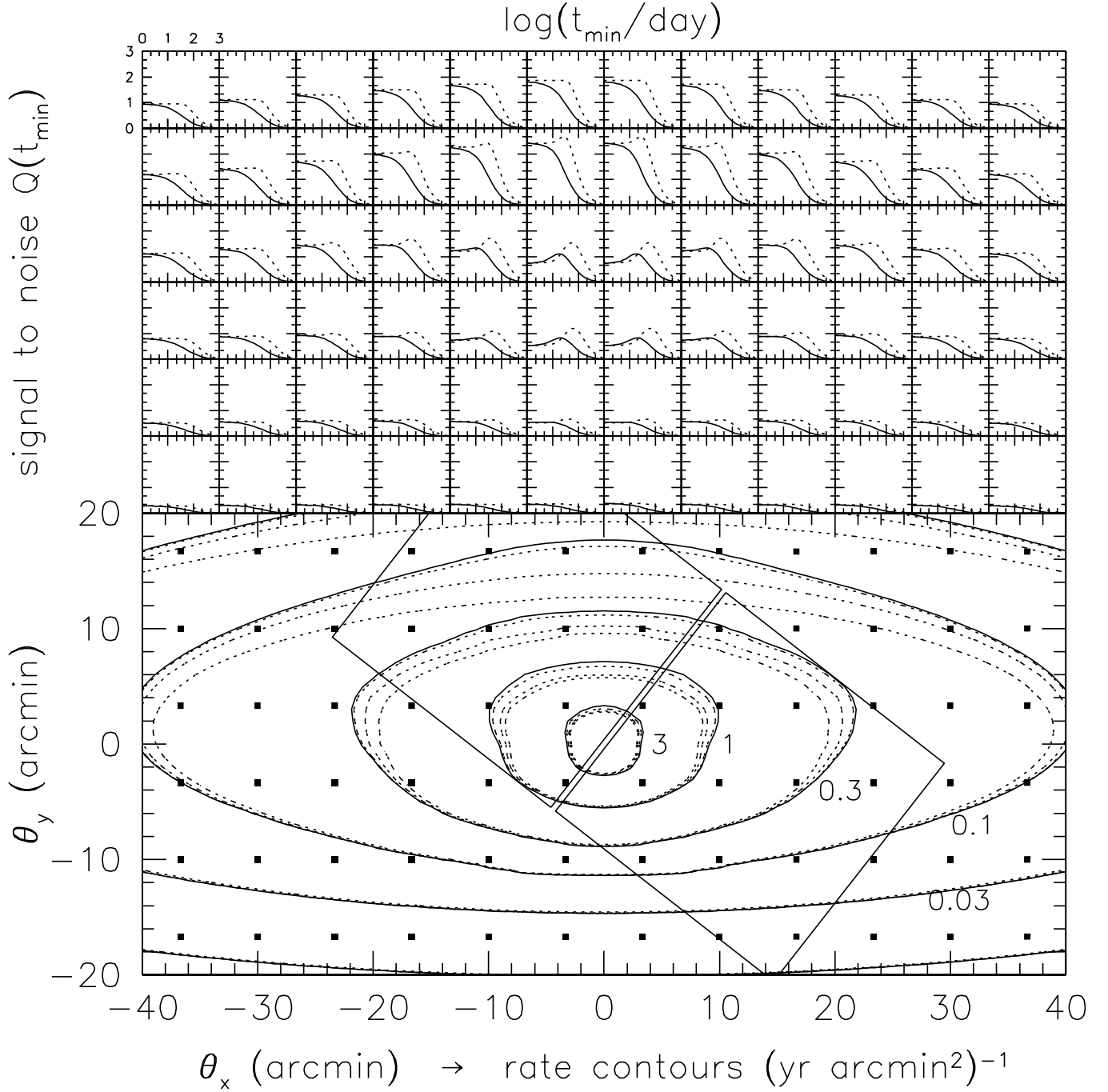


FIG. 5.— Rate contours for microlensing for different halo core radii (in units of events per year per square arcminute) and signal to noise for separating halo lensing from self lensing. The bottom panel illustrates the  $f_b = 0.2$ ,  $q = 1$  case, with solid contours indicating  $r_c = 1$  kpc, and the dotted contours indicate, moving inward,  $r_c = 2, 5, 10$  kpc respectively. There is a significant difference in rate towards the far end of the minor axis as the core radius varies, with the near end unaffected for the most part. The self lensing and Milky Way contributions are included. In the small top panels we illustrate the signal to noise (from Eq. 8) for separating a halo from self lensing for one year (three seasons) of observations over the box (about  $45 \text{ arcmin}^2$ ), taking a timescale cut at  $t_{\min}$ . Solid curves illustrate the cut in  $t_{1/2}$ , while the dotted curves illustrate the cut in  $t_E$ . The  $t_{1/2}$  cut doesn't help much, but if  $t_E$  is known, it is quite advantageous to make a cut near the center of the bulge.

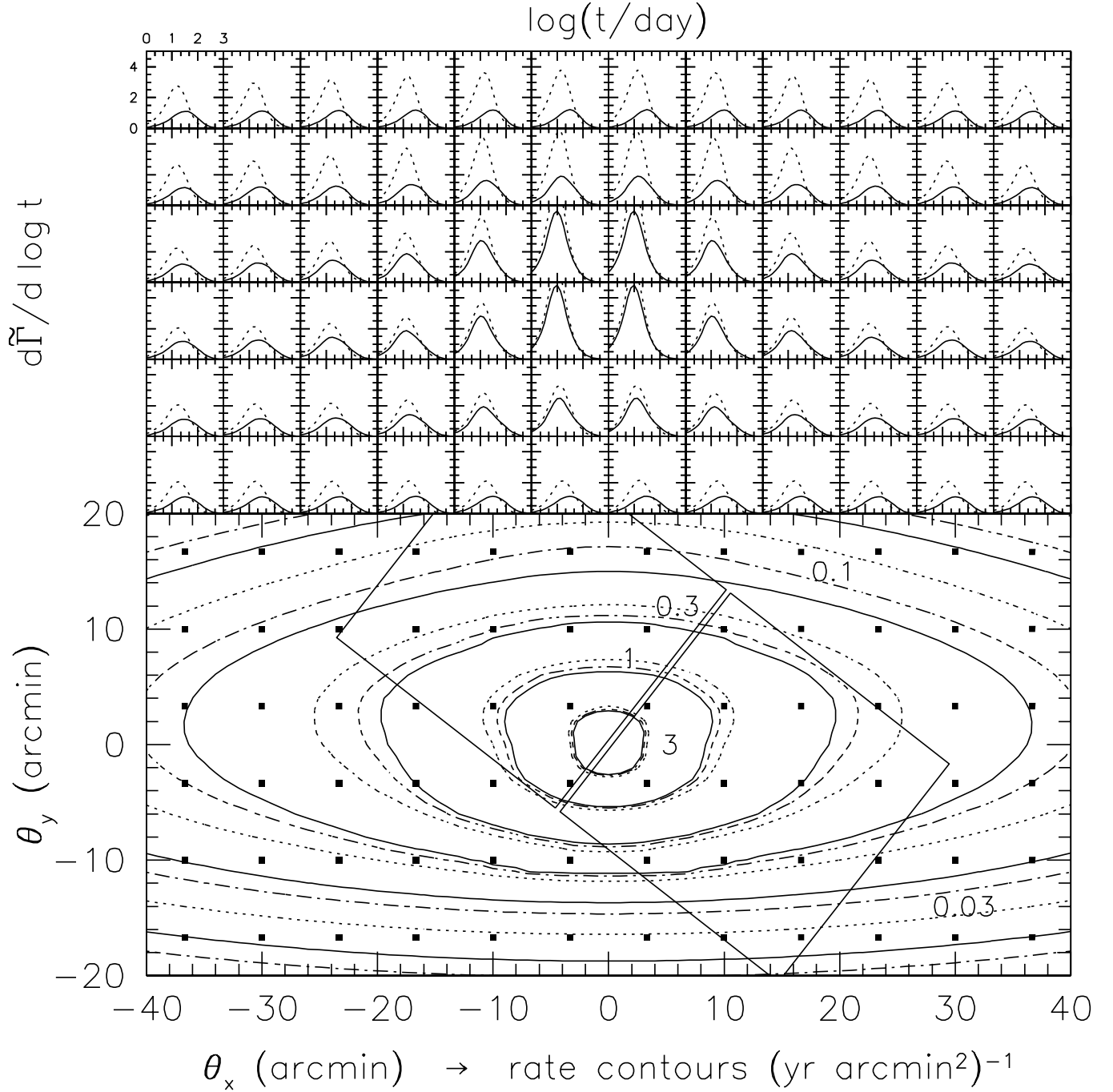


FIG. 6.— Rate contours for microlensing by lenses of different masses (in units of events per year per square arcminute) and rate distributions for two different halo lens masses. Self lensing and Milky Way contributions are included. The bottom panel illustrates the  $f_b = 0.2$ ,  $q = 1$ ,  $r_c = 2$  kpc case, with solid contours indicating a lens mass (for M31 and Milky Way halo contributions) of  $1.0M_\odot$ , dot-dashed contours indicating the fiducial case  $-3/8$  dex relative to solar, and the dotted contours indicating  $0.1M_\odot$  lenses. As expected, the rate for the lowest-mass lenses is the largest. In the top panels  $d\tilde{\Gamma}/d\log t_{1/2}$  is plotted for the  $0.1M_\odot$  (dotted curves) and  $1.0M_\odot$  (solid curves) cases, again normalized to unity at  $\log(\tilde{t}_{1/2}/\text{day}) = 1.75$  (about 56 days). In the center there is little difference, as the self lensing dominates. Away from the bulge, the longer timescales and lower rates of the heavier lenses is clearly seen.